

Ab initio calculations of mean free paths and stopping powers

A. P. Sorini,¹ J. J. Kas,¹ J. J. Rehr,¹ M. P. Prange,¹ and Z. H. Levine²

¹*Department of Physics, University of Washington, Seattle, WA 98195*

²*National Institute of Standards and Technology, Gaithersburg, Maryland 20899*

(Dated: September 17, 2018)

Abstract

A method is presented for first-principles calculations of inelastic mean free paths and stopping powers in condensed matter over a broad energy range. The method is based on *ab initio* calculations of the dielectric function in the long wavelength limit using a real-space Green's function formalism, together with extensions to finite momentum transfer. From these results we obtain the loss function and related quantities such as optical-oscillator strengths and mean excitation energies. From a many-pole representation of the dielectric function we then obtain the electron self-energy and inelastic mean free paths (IMFP). Finally using our calculated dielectric function and the optical-data model of Fernández-Varea *et al.*, we obtain collision stopping powers (CSP) and penetration ranges. The results are consistent with semi-empirical approaches and with experiment.

PACS numbers: 77.22.Ch; 34.80.-i; 34.50.Bw

I. I. INTRODUCTION

The effect of inelastic losses on fast electrons has long been of theoretical and experimental interest^{1,2,3}, and continues to be an area of active development^{4,5,6}. Theoretical calculations of such losses depend on the dielectric response of a material over a broad spectrum. Moreover, calculations of losses at low energies are particularly sensitive to the excitation spectrum of a material. While first-principles approaches have been developed for calculations of losses at low energies, i.e., up to a few tens of eV^{7,8}, these methods are computationally intensive and may be difficult to implement. Thus detailed calculations of inelastic losses have generally been limited to semi-empirical approaches^{4,9,10}, based on experimental optical data. On the other hand, experimental data over a sufficiently broad spectrum are not readily available for many materials of interest.

In an effort to overcome these difficulties, we present here a first-principles, real-space approach for general calculations of inelastic losses. The approach is applicable to both periodic and aperiodic condensed matter systems throughout the periodic table. Our calculations are based on *ab initio* calculations of the complex dielectric function $\epsilon(\omega) = \epsilon_1(\omega) + i\epsilon_2(\omega)$ in the long-wavelength limit, together with extensions to finite momentum transfer¹¹. The calculations of $\epsilon(\omega)$ are carried out using an all electron, real-space Green's function (RSGF) formalism as implemented in a generalization of the FEFF8 code^{12,13} for full-spectrum calculations of optical constants.

We focus in this paper on several physical quantities which characterize the inelastic interactions of a fast probe electron, a photo-electron, or other charged particle in condensed matter. These include the inelastic mean-free-path (IMFP) and the collision stopping-power (CSP). Each of these quantities depends on the complex dielectric function $\epsilon(\omega)$ through the loss function for a given material $-\text{[Im } \epsilon^{-1}(\omega)] = \epsilon_2(\omega)/[\epsilon_1(\omega)^2 + \epsilon_2(\omega)^2]$, which is calculated here up to x-ray energies. The loss function is directly related to the optical oscillator strength (OOS). From the OOS we obtain values of the mean excitation energy I which characterizes the distribution of excitations (e.g., plasmons, particle-hole excitations, etc.). Recently a comprehensive relativistic treatment of inelastic losses and scattering within the first Born approximation has been developed by Fernández-Varea *et al.*⁴. Their semi-empirical approach requires experimental optical data as input, and is referred to here as the optical data model (ODM). This approach has the advantage that calculations of quantities

such as the CSP are reduced to a single quadrature. To facilitate precise comparisons, we have used their formulation for our CSP calculations, except for the substitution of our *ab initio* dielectric function. Our approach is therefore referred to as the “*ab initio* data model” (ADM). We have also compared IMFPs calculated using both the ADM and a one-particle *self-energy* approach.

Formally the IMFP and the CSP are related to energy moments of the differential cross-section (DCS) for inelastic collisions $d\sigma/d\omega$ of a fast probe electron (or other charged particle) of initial kinetic energy E with energy loss ω . The inverse IMFP is proportional to the zeroth moment of the DCS

$$\frac{1}{\lambda(E)} = n_a \int d\omega \frac{d\sigma(\omega; E)}{d\omega} = n_a \sigma^{(0)}(E) , \quad (1)$$

where $n_a = N/V$ is the atomic number density. Here and elsewhere in this paper we use Hartree atomic units ($m = \hbar = e^2 = 1$). Thus distances are in Bohrs ($a_0 \approx 0.529 \text{ \AA}$) and energies in Hartrees ($H \approx 27.2 \text{ eV}$), unless otherwise specified. The CSP, here denoted by $S(E)$, is proportional to the first moment of the DCS

$$S(E) = n_a \int \omega d\omega \frac{d\sigma(\omega; E)}{d\omega} = n_a \sigma^{(1)}(E) . \quad (2)$$

Since $S(E) = -dE/dx$, this quantity has units of force. From an integral of $1/S(E)$ over energy we then obtain the net penetration range or path length $R(E)$. Implicit in Eqs. (1) and (2) are the kinematics of the colliding particles. In this paper we choose kinematics relevant for electrons, but we could alternatively use similar equations to describe protons or other ions by suitably modifying the domain of integration that defines $d\sigma/d\omega$ (see below). Regardless of the probe, the sample is characterized by the dielectric function $\epsilon(\mathbf{q}, \omega)$. In this paper we consider cubic materials which we approximate as isotropic, i.e., in which the dielectric function depends only on the magnitude of the momentum transfer $q = |\mathbf{q}|$.

The DCS may be considered as the sum of longitudinal (instantaneous Coulomb) and transverse (virtual photon) contributions, denoted below with subscripts L and T respectively. The detailed relativistic form of the relationship between each contribution to the DCS and the loss function is obtained by integrating the double differential cross-section (DDCS) over the kinematically allowed values of momentum-transfer⁴,

$$\frac{d\sigma(\omega; E)}{d\omega} = \int dq \frac{d\sigma(q, \omega; E)}{dq d\omega} , \quad (3)$$

where

$$\frac{d\sigma(q, \omega)}{dq d\omega} = \frac{d\sigma_L(q, \omega)}{dq d\omega} + \frac{d\sigma_T(q, \omega)}{dq d\omega}. \quad (4)$$

As an example of how the dielectric function determines the DDCS, we recall the familiar non-relativistic result:

$$\frac{d\sigma(q, \omega)}{dq d\omega} = \frac{d\sigma_L(q, \omega)}{dq d\omega} = -\frac{1}{2\pi n_a q v^2} \text{Im} \epsilon^{-1}(q, \omega). \quad (5)$$

The relativistic analog of Eq. (5) is similar and is given explicitly in Eqs. (8) and (9) of Ref.⁴.

One of the main goals of this work is to calculate mean excitation energies I and IMFPs for general condensed matter systems over an energy range up to about 100 keV. Another goal is to calculate CSPs and penetration ranges over a range of order 10 MeV. We compare our results both with other semi-empirical approaches and with experimental data and tabulations.

II. MODEL DIELECTRIC FUNCTION

Both the IMFP and the CSP can be computed as convolutions of the momentum-transfer and energy-loss dependent inverse dielectric function $\epsilon^{-1}(q, \omega)$, with relativistic weighting functions. The precise details of the weighting functions are discussed further below. In this Section we discuss the extension of our *ab initio* calculation of $\epsilon(q, \omega)$ in the long wavelength ($q \rightarrow 0$) limit to finite q ^{4,9,14,15,16}. In this work $\epsilon(\omega) \equiv \epsilon(0, \omega)$ is calculated from the UV to x-ray energies using the *ab initio* real-space Green's function code FEF8OP^{13,17}, which sums the contributions to the spectra over all occupied core and semi-core initial states. As an example, the calculated loss function for Ag is shown in Fig. 1.

We have chosen to discuss the extension to finite- q in terms of the loss function, but we could just as well have used the OOS $g(\omega)$, which differs by a factor proportional to ω , i.e.,

$$g(\omega) = -\frac{2}{\pi} \frac{Z}{\Omega_p^2} \omega \text{Im}[\epsilon^{-1}(\omega)], \quad (6)$$

where $\Omega_p^2 = 4\pi n_a Z$ is the all-electron plasma frequency. As an illustration of the quantitative agreement of our approach, three *ab initio* OOS calculations, spanning a range of atomic numbers, are compared to experiment in Fig. 2. Clearly the approximations in FEF8 such as the use of atomic core initial states in the OOS calculation and muffin-tin scattering

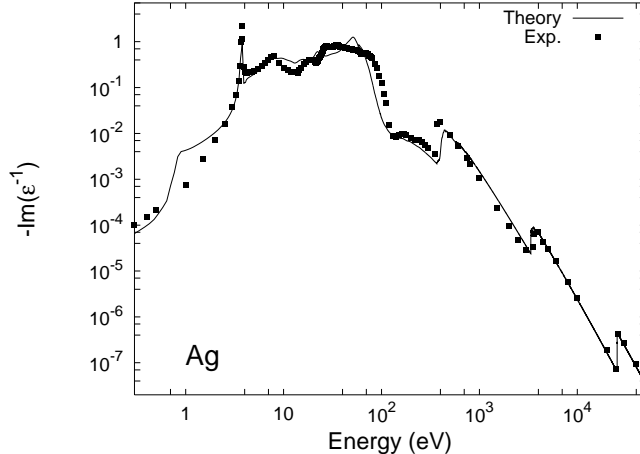


FIG. 1: Loss function $-\text{Im} \epsilon^{-1}(\omega)$ of fcc silver as calculated in this work (solid line) and from experiment^{18,19} (dots).

TABLE I: Mean excitation energies for several elements as calculated in this work, and for comparison, results calculated from experimental^{19,21} optical constants, and recommended (ICRU²²) values.

| Element | I theory (eV) | I expt (eV) | ICRU (eV) |
|----------|-----------------|---------------------------------------|-----------|
| Aluminum | 165 | 167 ²¹ , 162 ¹⁹ | 166 |
| Silicon | 174 | 173 ²¹ | 173 |
| Copper | 312 | 319 ¹⁹ | 322 |
| Silver | 420 | 382 ¹⁹ | 470 |
| Gold | 662 | 752 ¹⁹ | 790 |

potentials are adequate to yield good agreement with experiment for UV energies and above. Additional examples are tabulated on the WWW²⁰. For optical frequencies and below, however, the agreement is only semi-quantitative, but the errors tend to be suppressed in the OOS due to the overall factor of ω in Eq. (6).

A global measure of the excitation spectra is given by the “mean excitation energy” $\ln I = \langle \ln \omega \rangle$, where the “mean” $\langle \dots \rangle$ refers to an average with respect to the OOS weighting function, i.e.,

$$\ln I = \frac{\int d\omega g(\omega) \ln \omega}{\int d\omega g(\omega)}. \quad (7)$$

The quantity I appears in expressions for the collision stopping power, as shown in Sec. V. below. In Table I theoretical values of I , as calculated from our OOS spectra, are compared

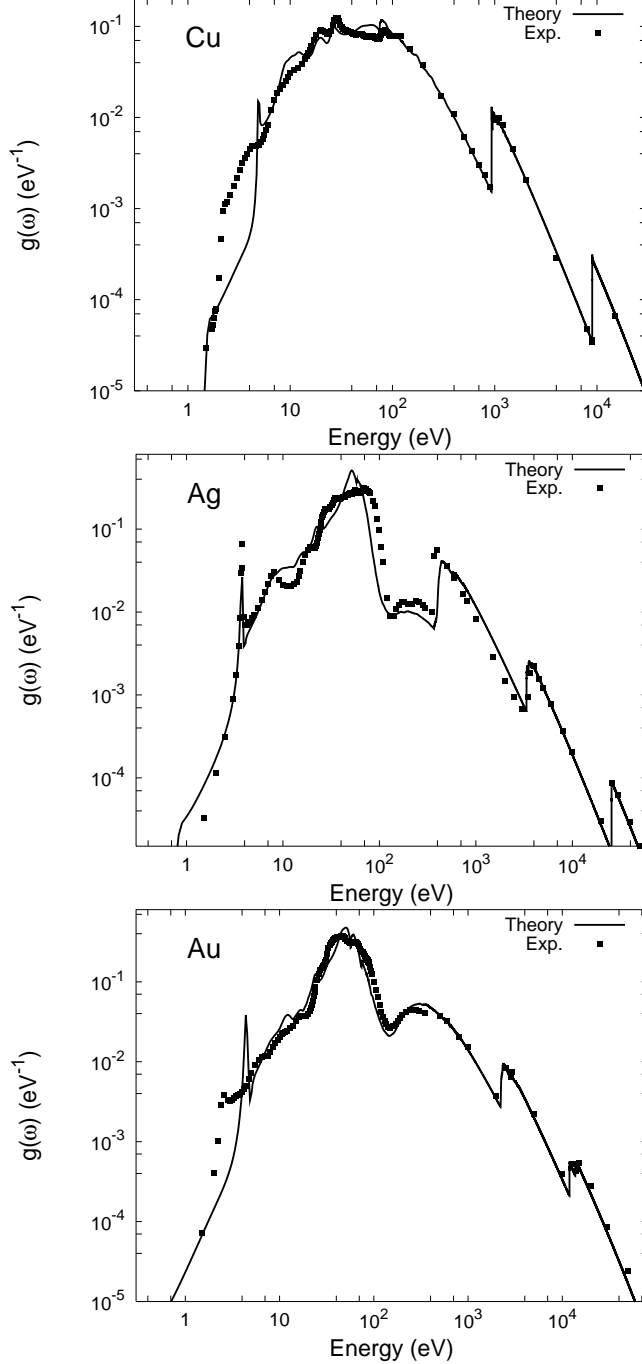


FIG. 2: Optical oscillator strengths for a) Cu (upper), b) Ag (middle) and c) Au (lower) as calculated in this work (solid) using the FEFF8OP code and compared to experiment^{18,19} (points).

with those calculated from experimental optical constants¹⁹, and also with internationally recommended (ICRU) values for several elements. For low Z elements, the theoretical values of I are clearly in good agreement with measured values. For high Z elements I is predicted by Thomas-Fermi models to be proportional to Z . The proportionality constant can be

determined experimentally to give a semi-empirical “rule of thumb” $I \approx 10 Z$ (eV). In the high Z regime the agreement between theory and experiment appears to be only semi-quantitative, but it should be mentioned that the ratio of I to Z is not in fact constant but rather it varies from around 9 to around 11 and has been measured to be as low as 8.32 for lanthanum²³. Furthermore, only the logarithm of I is needed for the determination of physical quantities, and typical errors in $\ln I$ from the values in in Table I are only a few percent. For example, for the case of 100 keV electrons in gold, the error in stopping powers calculated using experimental versus theoretical values of I is only around 2%.

In the IMFP calculations presented here we consider two different extensions to finite q , as described below. Since our calculations show that both lead to similar results for the IMFP, we only present calculations of the CSP with one of these extensions. However, all our calculations use the same full-spectrum calculations of $\epsilon(\omega)$. For our IMFP calculations, we have used the many-pole representation of the dielectric function of Ref.¹¹, i.e. we approximate our calculated loss function $-\text{Im}[\epsilon^{-1}(\omega)]$ as a sum of many (typically of order 100) discrete poles. This “many-pole” model, denoted by $\epsilon_N^{-1}(\omega)$, has the standard analytic form for dielectric response,

$$\epsilon_N^{-1}(\omega) = 1 + \sum_{j=1}^N g_j \frac{\omega_j^2}{\omega^2 - \omega_j^2 + i\omega\delta}, \quad (8)$$

where $\delta\omega$ is a small damping term, comparable to the pole separations. Fig. 3 compares the IMFP for Cu as calculated using both our many-pole model and a single plasmon-pole model²⁴. This single-pole model is essentially an Einstein-model for the response in which excitations (for a given momentum transfer q) occur at the plasmon excitation energy ω_q . Thus the single-pole model is a special case of the many-pole model in which all but one of the weights g_j appearing in Eq. (8) are set to zero. In our many-pole representation, the parameters ω_j are taken to be evenly spaced along the energy-loss axis, and the weights g_j are fixed by matching our calculation of $\text{Im}[\epsilon^{-1}(\omega)]$ according to the formula

$$g_j = -\frac{2}{\pi} \frac{1}{\omega_j^2} \int_{\Delta_j} d\omega \omega \text{Im}[\epsilon^{-1}(\omega)], \quad (9)$$

where the integration region Δ_j is from $(\omega_j + \omega_{j-1})/2$ to $(\omega_j + \omega_{j+1})/2$ and the similarity with Eq. (6) is apparent. Finally, the extension to finite q is obtained by shifting the pole locations via the substitution²⁴

$$\omega_j^2 \rightarrow \omega_j^2 + \frac{v_F^2 q^2}{3} + \frac{q^4}{4}, \quad (10)$$

where $v_F = k_F/m$ is the Fermi velocity as calculated at the mean interstitial electron density from the FEFF8 code. Further details of our approach, though not essential to our discussion here, are given in Refs.^{11,17} and²⁵. The above substitution is sufficient to induce the so-called “Bethe ridge” for large momentum-transfer where the loss function is peaked about the point $\omega = q^2/2$. In other words, our model for large q satisfies the approximate relation

$$-\text{Im}[\epsilon^{-1}(q, \omega)] \approx \pi \Omega_p^2 \delta(\omega^2 - Q^2), \quad (11)$$

where $Q \equiv q^2/2$. Consequently the above extension can be regarded as an interpolation formula between small and large Q .

For CSP calculations, our aim here is to replace experimental optical data (which is used as input in the ODM of Ref.⁴) with theoretical “optical data” from our *ab initio* calculation of $\epsilon(\omega)$, i.e., with an *ab initio* data model (ADM). Thus for consistency we follow the formulation of Ref.⁴ as closely as possible in comparisons with their CSP results, In particular we have also implemented their delta-oscillator^{14,26} extension to finite q for our CSP calculations. For non-relativistic probe electrons the delta-oscillator model extends $\epsilon(\omega)$ to finite q according to the relation

$$\begin{aligned} -\text{Im}[\epsilon^{-1}(q, \omega)] &= \pi \Omega_p^2 \frac{Z(Q)}{Z} \delta(\omega^2 - Q^2) \\ &\quad - \text{Im}[\epsilon^{-1}(\omega)] \theta(\omega - Q), \end{aligned} \quad (12)$$

where $Z(Q)$ is the number of electrons that contribute to the zero momentum-transfer sum-rule with upper energy limit Q ,

$$Z(Q) = -\frac{2Z}{\pi \Omega_p^2} \int_0^Q d\omega \omega \text{Im}[\epsilon^{-1}(\omega)]. \quad (13)$$

Because $Z(Q)$ approaches Z for large q we see that the extension to finite q in Eq. (12) gives the Bethe ridge in much the same way as that of Eq. (11). Although the finite- q extension algorithms in this paper differ somewhat, we do not expect our non-relativistic results to depend significantly on the details. The reason is that both algorithms reduce to the correct long-wavelength limit for low q , and both give the correct Bethe ridge dispersion for high q . This expectation is supported by the IMFP results in Sec. IV. Moreover our results for the q dependence are roughly consistent with the explicit real space calculations of $-\text{Im}[\epsilon^{-1}(q, \omega)]$ at finite q of Soininen et al.²⁷.

III. III. ELECTRON SELF-ENERGY

Inelastic losses in the propagation of a fast charged particle can be expressed in terms of one-particle *self-energy* $\Sigma(E)$. This complex-valued quantity is a dynamically screened exchange-correlation contribution to the quasi-particle energy-momentum relation

$$E = \frac{p^2}{2} + \Sigma(E), \quad (14)$$

where p is the quasi-particle momentum. Our approach for calculating $\Sigma(E)$ is based on the “*GW*” approximation of Hedin²⁸, together with our many-pole representation of the dielectric function, as summarized above¹¹. In the *GW* method the vertex-corrections to the electron self-energy are neglected, yielding an expression for $\Sigma(E)$ in terms of the electron propagator G and the screened Coulomb potential acting on an electron W , i.e.,

$$\Sigma(E) = i \int \frac{d\omega}{2\pi} e^{-i\omega\eta} G(E - \omega) W(\omega), \quad (15)$$

where η is a positive infinitesimal and spatial indices (\mathbf{x}, \mathbf{x}') have been suppressed for clarity. Within the RSGF approach, the propagator G is calculated using a multiple-scattering expansion $G = G_0 + G_0 t G_0 + \dots$ ¹². However, for simplicity in this work, we neglect the multiple-scattering terms (which would give rise to fluctuations in the self-energy) and simply use the free propagator G_0 for a homogeneous electron gas at the mean interstitial density. Then the screened Coulomb interaction for a spatially homogeneous system can be obtained from the Fourier transform $W(\mathbf{q}, \omega) = \mathcal{F}[W(\mathbf{x} - \mathbf{x}', t)]$ and can be expressed in terms of the Coulomb potential $v_q = 4\pi/q^2$ and the dielectric function $\epsilon(\mathbf{q}, \omega)$ as:

$$W(\mathbf{q}, \omega) = \epsilon^{-1}(\mathbf{q}, \omega) v_q. \quad (16)$$

The calculations of $\Sigma(E)$ are then carried out using the many-pole representation of Eq. (8) and (10). With this homogeneous model, our calculated $\Sigma(E)$ is then the average self-energy in the system. Further details are given in Ref.²⁵.

IV. IV. INELASTIC MEAN FREE PATH

We first calculate Eq. (1) for the IMFP in terms of the excited state *self-energy* $\Sigma(E)$ of the fast electron.

$$\lambda(E) = \sqrt{\frac{E}{2}} \frac{1}{|\text{Im} \Sigma(E)|}. \quad (17)$$

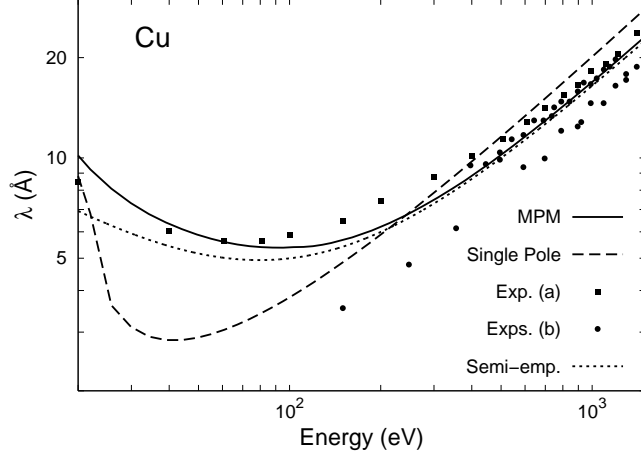


FIG. 3: Inelastic mean free paths for copper calculated using the same *ab initio* dielectric function as the basis of two different theoretical models: The many-pole self-energy (MPM) model of Eq. (17) and the single-pole self-energy model (described in the text). These theoretical results are compared to: Exp. (a)²⁹ (squares), Exps. (b) (circles, the references for Exps. (b) are given in Ref.⁵), and a semi-empirical curve which is described in Ref.⁵.

Eq. (17) for the IMFP is consistent with the decay of a single electron wavefunction whose time dependence is given by $e^{-iE(p)t}$ ³¹. Eq. (17) is also equivalent to Eq. (1), because the self-energy is proportional to the forward scattering amplitude, i.e.,

$$\text{Im } \Sigma(\mathbf{p}) = -2\pi n_a \text{Im } f(\mathbf{p}, \mathbf{p}), \quad (18)$$

i.e., the equivalence of Eq. (1) and Eq. (17) follows from the optical theorem.

The explicit dependence of the self-energy on the dielectric function in Eq. (16), the many-pole model of Eq. (8), and (10), and the full-spectrum FEFF8OP code are all that are needed to carry out *ab initio* calculations of IMFPs according to Eq. (17). Our many-pole model IMFP calculations (labeled MPM) are shown for several materials in Figs. 3 and 4, together with best fits⁵ to currently available data. The fit lines in Figs. 3 and 4 are based on multiple data sets which were taken up to 3000 eV and are expected to accurately describe the IMFP as low as 50 eV. Fig. 4 also shows a calculation (labeled “ADM”) which uses our *ab initio* $\epsilon(\omega)$ as input data to the semi-empirical optical-data model of Ref.⁴. Note that the MPM and ADM results are in in good agreement with each other, which verifies that the different extensions to finite q discussed in Sec. II. do not lead to significantly different results. Both theoretical models are plotted here over the expected range of validity of the fit line, but can be extended with our codes to energies up to about 100 keV. Although

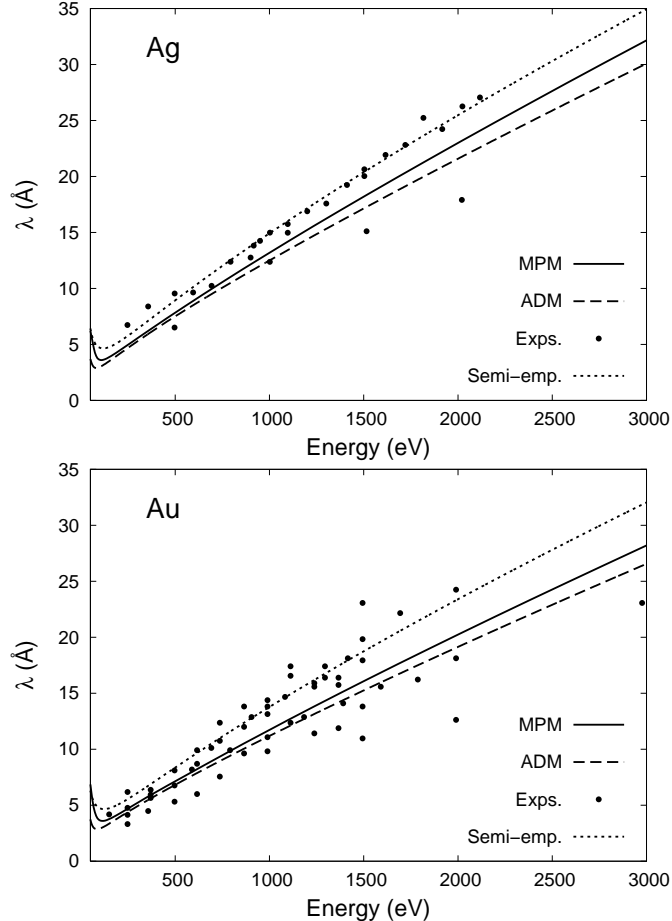


FIG. 4: Inelastic mean free paths for a) silver (upper) and b) gold (lower) calculated using the same *ab initio* dielectric function as the basis for two different theoretical models: the many-pole self-energy (MPM) model of Eq. (17), and the “*ab initio* data” model (ADM) described in the introduction. The theoretical results are compared to a semi-empirical curve⁵ and to multiple experimental data sets. The references for the Exps. are given in Ref.⁵. The theoretical models are plotted over the expected range of validity of the semi-empirical curve.

the agreement with experiment is reasonable, our calculations tend to underestimate the experimental IMFP somewhat for high Z materials.

V. STOPPING POWER

As noted in the introduction the CSP is the net reaction force $S(E) = -dE/dx$ due to electronic collisions at a given energy E that slows a fast probe electron. Over the range of energies from about 10 eV up to about 10 MeV the CSP is the main contribution to the

total stopping power. Above this energy the total stopping power may be dominated by bremsstrahlung. The CSP is calculated in this work using Eq. (2), where the DCS is related to our *ab initio* loss function using the formulation of Ref.⁴. This model is thought to be applicable with confidence for energies above about 100 eV, and appears to be applicable as low as about 10 eV. However, it is not obvious why a model based on the first Born approximation should be valid at such low energies. In the relativistic limit Eq. (2) reduces to the well-known Bethe-formula^{1,2,3,32} for the stopping power

$$S(E) = \frac{\pi \Omega_p^2}{2 v^2} \left[\ln \left(\frac{E^2 \gamma + 1}{I^2} \frac{\gamma + 1}{2} \right) + F(\gamma) - \delta_F(\gamma) \right], \quad (19)$$

where $\gamma = (1 - v^2/c^2)^{-1/2}$ is the relativistic dilation factor, and $F(\gamma)$ is given by

$$F(\gamma) = \left[\frac{1}{\gamma^2} - \frac{2\gamma - 1}{\gamma^2} \ln 2 + \frac{1}{8} \left(\frac{\gamma - 1}{\gamma} \right)^2 \right]. \quad (20)$$

Also appearing in Eq. (19) are the “mean excitation energy” I defined in Sec. II., and Fano’s density correction³ δ_F . The density correction δ_F is due solely to transverse interactions, and can be neglected for non-relativistic particles. A detailed description of how δ_F can be calculated as a functional of the loss function, is given in Ref.⁴. Fig. 5 shows the density correction $\delta_F(E)$ for copper as calculated using our *ab initio* dielectric function, and for comparison, the semi-empirical values used by ESTAR³³. ESTAR is an on-line implementation of Eq. (19) which semi-empirical values of I as input. The mean excitation energy and the density correction have, heretofore, been difficult to calculate from first-principles, as they require accurate values of the OOS over a very large energy spectrum. However, our full-spectrum approach clearly gives reasonable agreement with experiment.

For relativistic probe particles, the excellent agreement of the Bethe formula in Eq. (19) for the CSP is well known, so we have included data from ESTAR in lieu of experiment where necessary. The difference between Eq. (19) and Eq. (2) only appears in the non-relativistic regime, and can be seen in Fig. 6, where Eq. (19) begins to fail around 5000 eV. In order to calculate CSPs that are in good agreement with experiment for both non-relativistic and relativistic probe electrons we apply Eq. (2) with the more general form of $d\sigma/d\omega$ given in Ref.⁴, but using our calculated dielectric function as input.

Figs. 6 and 7 show that the calculated CSPs for high energy electrons for the systems studied here (Cu, Ag and Au) are in good agreement with the ESTAR results. For lower

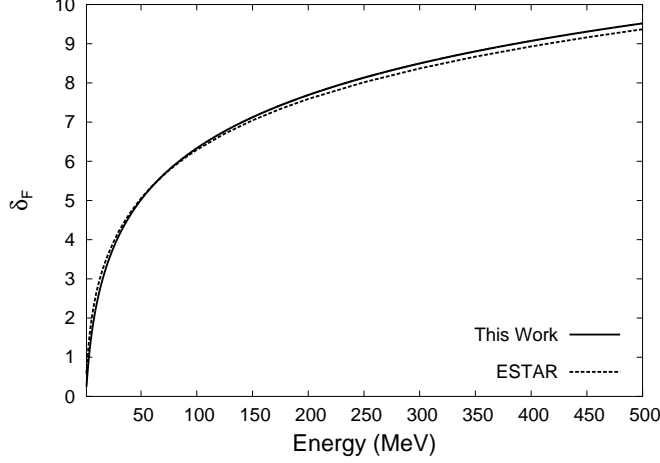


FIG. 5: Fano's density effect correction to the stopping power from Eq. (19) as calculated in this work (solid), and compared to semi-empirical values³³ for copper (dashes).

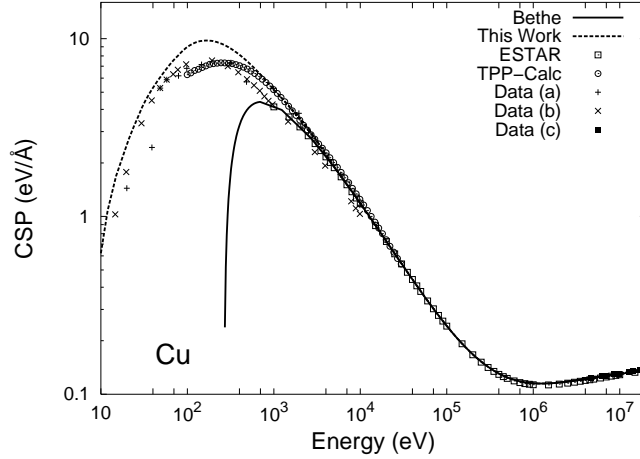


FIG. 6: Collision stopping power for copper as calculated using the *ab initio* dielectric function of this work (dashes) in the ADM (see text). Also shown are semi-empirical values of the CSP from ESTAR³³ (open squares), and semi-empirical CSP values (labeled TPP-calc) based on the Penn model³⁰ (circles), and CSP values from experimental data: (+)³⁴, (x)³⁵, and (solid squares)³⁶.

energies the CSP calculations of this work show significantly better agreement with data than the Bethe formula.

It is interesting to note that the CSP falls off approximately as a power-law of the energy over a few decades beyond the peak loss, but before the transverse effects take over. Because of this, the range $R(E)$ defined by

$$R(E) = \int_0^E \frac{dE}{S(E)}, \quad (21)$$

is also well approximated as a power-law. This approximate power-law dependence of $R(E)$

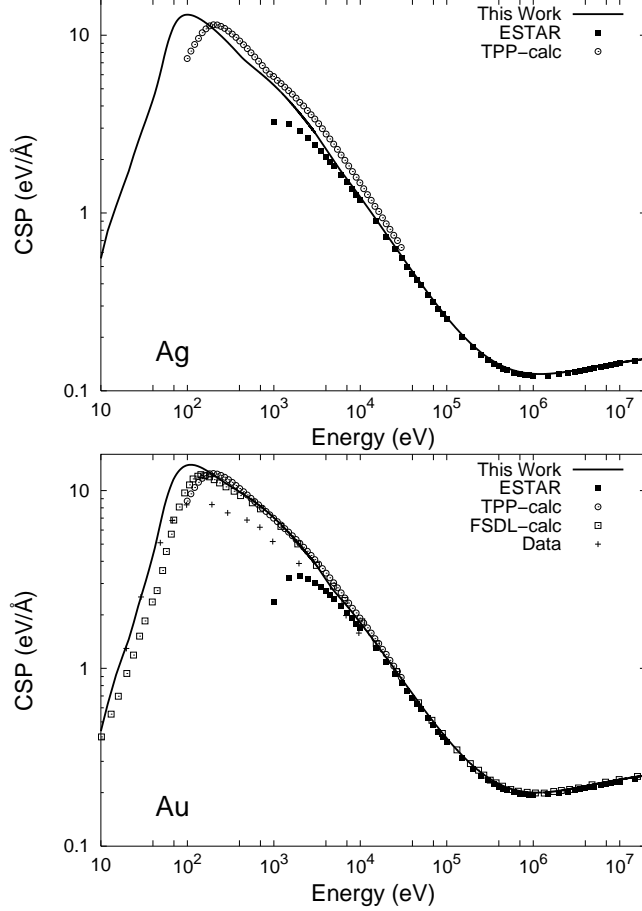


FIG. 7: Collision stopping powers for a) Ag (upper) and b) Au (lower), with labels as in Fig. 6. Also shown for Au are the semi-empirical CSP values as calculated in Ref.⁴ (labelled FSDL-calc), and CSP values from experiment³⁴.

is shown in Fig. 8 for silver, and compared with our full calculation and ESTAR.

VI. VI. CONCLUSIONS

We have presented a general real-space Green's function approach for *ab initio* calculations of inelastic losses and stopping powers in condensed matter. Unlike most current approaches, our method is based on *ab initio* calculations of dielectric response, and does not rely on empirical optical data. We find that our many-pole self-energy model, which is derived from our many-pole dielectric function, yields inelastic mean free paths in better agreement with experimental data than the single-pole plasmon model. Thus our many-pole self-energy more accurately accounts for inelastic losses in various electron and x-ray spectroscopies than the single plasmon-pole self-energy. We also find that accurate calculations of inelastic losses

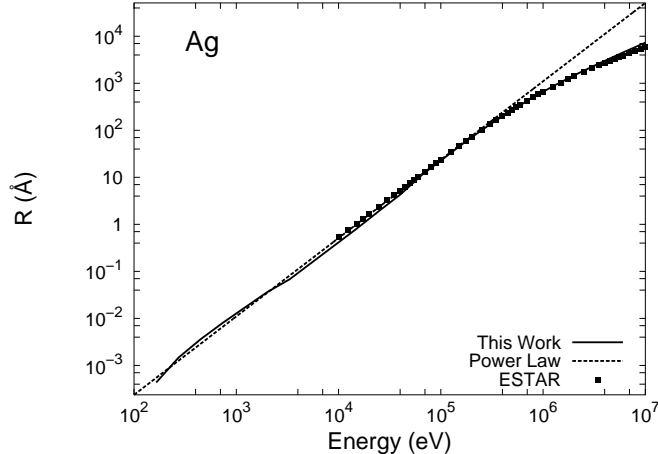


FIG. 8: The range $R(E)$ as given by Eq. (21) of electrons in silver as calculated in this work (solid) and compared to ESTAR (squares) and to a pure power-law $R(E) = 0.271E^{5/3}$ (dashes) with E in Hartrees.

depend primarily on the quality of the calculated $q = 0$ dielectric function, and not on the details of the extension to finite q . Using our *ab initio* dielectric function, we also calculate the mean excitation energy and thus stopping powers for relativistic electrons, obtaining results in good agreement with experimental data. Furthermore, using the *ab initio* ADM we can extend the stopping power calculation down to energies of $O(10)$ eV, i.e., much lower than the Bethe formula, while still maintaining reasonable agreement with experiment. Our approach for calculating stopping powers of electrons can be extended to protons and other ions by suitably modifying the kinematics. We have also found that the net range (or path length) $R(E)$ can be represented as a power law over several decades of energy. That such a simple analytic description of the range of probe electrons in a solid exists is interesting and also could be useful for reducing computation times in Monte Carlo calculations used to study radiation damage and in other applications where numerous electron energy-loss tracks need to be considered. In conclusion, we believe our approach has the potential to complement or provide an alternative to semi-empirical approaches for calculations of IMFPs and stopping powers in condensed matter.

VII. ACKNOWLEDGMENTS

We wish to thank G. Bertsch, H. Bichsel, J. Fernández-Varea, C. Powell, P. Rez, and E. Stern for comments and suggestions. This work is supported in part by the DOE Grant

DE-FG03-97ER45623 (JJR) NIH NCCR BTP Grant RR-01209 (JJK), and NIST Grant 70 NAMB 2H003 (APS) and was facilitated by the DOE Computational Materials Science Network.

- ¹ H. A. Bethe, *Ann. Phys.* **5**, 325 (1930), this paper is reviewed in Ref.³².
- ² E. Fermi, *Phys. Rev.* **57**, 485 (1940).
- ³ U. Fano, *Ann. Rev. Nucl. Sci.* **13**, 1 (1963).
- ⁴ J. M. Fernández-Varea, F. Salvat, M. Dingfelder, and D. Liljequist, *Nucl. Instr. and Meth. B* **229**, 187 (2005).
- ⁵ C. J. Powell and A. Jablonski, *J. Phys. Chem. Ref. Data* **28**, 19 (1999).
- ⁶ H. Bichsel, in *Atomic, Molecular, and Optical Physics Handbook*, edited by G. W. F. Drake (AIP Press, Woodbury, N.Y., 1996).
- ⁷ I. Campillo, J. M. Pitarke, A. Rubio, E. Zarate, and P. M. Echenique, *Phys. Rev. Lett.* **83**, 2230 (1999).
- ⁸ J. A. Soininen, J. J. Rehr, and E. L. Shirley, *J. Phys.: Condens. Matter* **15**, 2572 (2003).
- ⁹ D. R. Penn, *Phys. Rev. B* **35**, 482 (1987).
- ¹⁰ R. M. Sternheimer, S. M. Seltzer, and M. J. Berger, *Phys. Rev. B* **26**, 6067 (1982).
- ¹¹ J. J. Rehr, J. J. Kas, M. P. Prange, F. D. Vila, A. L. Ankudinov, L. W. Campbell, and A. P. Sorini, arXiv:cond-mat/0601242, 2006, unpublished.
- ¹² A. L. Ankudinov, B. Ravel, J. J. Rehr, and S. D. Conradson, *Phys. Rev. B* **58**, 7565 (1998).
- ¹³ M. Prange, G. Rivas, J. Rehr, and A. Ankudinov, unpublished.
- ¹⁴ D. Liljequist, *J. Phys. D: Appl. Phys.* **16**, 1567 (1983).
- ¹⁵ J. C. Ashley, J. J. Cowan, R. H. Ritchie, V. E. Anderson, and J. Hoelzl, *Thin Solid Films* **60**, 361 (1979).
- ¹⁶ J. C. Ashley, *J. Electron Spectrosc. Relat. Phenom.* **46**, 199 (1988).
- ¹⁷ M. Prange, G. Rivas, and J. J. Rehr, *Table of Optical Constants for Mg, Al, Cu, Ag, Au, Bi and C*. (World Wide Web, <http://leonardo.phys.washington.edu/feff/opcons/>, 2005).
- ¹⁸ H. J. Hagemann, W. Gudat, and C. Kunz, *J. Opt. Soc. Am.* **65**, 7421 (1975).
- ¹⁹ H. J. Hagemann, W. Gudat, and C. Kunz, *Optical Constants from the Far Infrared to the X-ray Region: Mg, Al, Cu, Ag, Au, Bi, C and Al₂O₃*, DESY SR-7417 (Desy, Hamburg, W. Germany,

- 1974).
- ²⁰ A. P. Sorini, J. Kas, J. J. Rehr, and M. P. Prange, *Tables of mean free paths and stopping powers*. (World Wide Web, <http://leonardo.phys.washington.edu/feff/loss/>, 2005).
- ²¹ C. Tschalar and H. Bichsel, *Phys. Rev.* **175**, 476 (1968).
- ²² ICRU, *ICRU Report 37, Stopping Powers and Ranges for Protons and Alpha Particles*. (International Commission of Radiation Units and Measurements., 1984).
- ²³ H. Bichsel, *Phys. Rev. A* **46**, 5761 (1992).
- ²⁴ B. Lundqvist, *Phys. Kondens. Materie* **6**, 193 (1967).
- ²⁵ J. Kas, A. Sorini, M. Prange, and J. Rehr, unpublished.
- ²⁶ F. Salvat, J. M. Fernández-Varea, and J. Sempau, *PENELOPE - A Code System for Monte Carlo Simulation of Electron and Photon Transport* (OECD/Nuclear Energy Agency, Issy-les-Moulineaux, France, <http://www.nea.fr>, 2003).
- ²⁷ J. A. Soininen, A. L. Ankudinov, and J. J. Rehr, *Phys. Rev. B* **72**, 045136 (2005).
- ²⁸ L. Hedin and S. Lundqvist, *Solid State Phys.* **23**, 1 (1969).
- ²⁹ W. S. M. Werner, *Surf. Interface Anal.* **31**, 141 (2001).
- ³⁰ S. Tanuma, C. J. Powell, and D. R. Penn, *Surf. Interface Anal.* **37**, 978 (2005).
- ³¹ J. J. Quinn, *Phys. Rev.* **126**, 1453 (1962).
- ³² M. Inokuti, *Rev. Mod. Phys.* **43**, 297 (1971).
- ³³ M. J. Berger, J. S. Coursey, M. A. Zucker, and J. Chang, *ESTAR, PSTAR, and ASTAR: Computer Programs for Calculating Stopping-Power and Range Tables for Electrons, Protons, and Helium Ions (version 1.2.3)* (National Institute of Standards and Technology, Gaithersburg, MD., <http://physics.nist.gov/Star>, 2005).
- ³⁴ S. Luo, X. Zhang, and D. C. Joy, *Radiat. Eff. Def. Solids* **117**, 235 (1991).
- ³⁵ P. Hovington, D. C. Joy, R. Gauvin, and N. Evans, *Scanning Microsc.* **10**, 653 (1996).
- ³⁶ M. S. Macpherson, Ph.D. thesis, NRC Report PIRS-0626 (1998).